

# Analytical and Numerical Study of FRP Retrofitted RC Beams Under Low Velocity Impact

M.Z. Kabir<sup>1,\*</sup> and E. Shafei<sup>1</sup>

**Abstract.** *An analytical along with numerical analysis has been carried out to investigate the behavior of concrete simply supported beams strengthened with Fiber-Reinforced Polymer (FRP) unidirectional laminates under impact loading. Concrete beams are reinforced with a minimum ratio of flexural and shear steel rebars and finally retrofitted with epoxy-bonded high strength carbon FRP laminates in their flexure surfaces. The impact force was applied with a solid steel cylinder drop weight. Analytical results showed that composite laminates externally bonded to reinforced concrete beam substrate can significantly enhance the performance of these structural members to resist impact loadings. Also, based on the obtained results, in retrofitted beams the crack propagation happens in a desirable mode; an increasing of yielded rebar zones and residual beam stiffness. Retrofitted beams were stiffer than unretrofitted ones in their first impact response. The residual stiffness of impacted concrete beams depends on their initial stiffness and the impact energy level. The analytical method uses an idealized elastic spring-mass model and flexural wave propagation theory to calculate the dynamic response of assumed beams. Analytical responses are adjusted due to an inelastic response, and finally are used for the simplified designation of impact resisting reinforced concrete beams retrofitting laminates.*

**Keywords:** *Impact loading; Reinforced concrete beam; Composite laminate; Retrofitting; FEM.*

## INTRODUCTION

In practical cases, reinforced concrete structures can be subjected to sudden dynamic impacts, like drop projectile impacts, blasts and ocean waves. The main characteristics of impact load are a high loading rate and a very short period of application that results in high material strain rates. Meanwhile, the mechanical behavior of structural materials can be changed due to high strain rates too. So, traditional static analysis methods cannot be used as a solution to this complex case. This subject has been paid attention to by many engineers in recent past years.

Projectile induced impacts can be classified as low velocity and high velocity according to the projectile mass and velocity. As a general view, a low-mass

projectile at high velocity may cause a high velocity impact, but a high-mass projectile at low velocity can cause a low velocity impact. This paper investigates the retrofitting effect of unidirectional composite laminates in controlling the structural behavior of reinforced concrete beams subjected to low velocity impacts.

The advantages of laminated composites like high strength-to-weight ratio, high tensile rupture strength and their easy application procedures cause their frequent usage in civil and mechanical engineering projects. Composite laminates are almost fabricated with carbon, glass and aramid fibers bonded with epoxy or other thermo-set resins and have various ply lay-up configurations. Carbon-based composite laminates (CFRP) have a high tensile modulus and strength and can service well in high temperature fields. Aramid and glass-based laminates (KFRP and GFRP) have lower strength and tensile strengths but higher failure strain values. All the above-mentioned laminate types can be quite suitable for the impact retrofitting of concrete structures. Most laminated fiber-reinforced

1. Department of Civil and Environmental Engineering, Amirkabir University of Technology, Tehran, P.O. Box 15875-4413, Iran.

\*. Corresponding author. E-mail: mzkabir@aut.ac.ir

Received 11 October 2008; received in revised form 12 February 2009; accepted 16 March 2009

composites behave in a linearly elastic regime up to their ultimate failure rupture limit.

In recent years, much research has been undertaken in the FRP-based retrofitting of concrete structures to resist static and earthquake loadings, but relatively few studies have been done on the retrofitting of these members to withstand sudden and impact loadings.

**RESEARCH SIGNIFICANCE**

The lack of strength in traditional reinforced concrete members against impact loading has been considered extremely important during last few years. The absorbed impact energy, local and global response of these structures can severely affect their designation procedure. The main objective of this paper is to give a general view about the behavior of unretrofitted reinforced concrete beams subjected to low velocity impact loading and their performance changes when subjected under retrofitting using composite unidirectional laminates. The variations of stiffness, deflection, absorbed impact energy, crack modes, yielded zones of steel rebars and probable debonding interfaces are taken into account as investigated parameters. Based on the numerical simulation results and mathematical manipulations, the total reaction force and maximum deflection can be estimated in an appropriate manner.

**EXISTING LITERATURES**

Erki and Meier [1] investigated the impact behavior of four 8-meter reinforced concrete beams retrofitted with steel plates and Kevlar sheets (KFRP) in an experimental case. The impact load was induced by lifting one end of a simply supported beam and dropping it from given heights. Comparisons are made between the dynamic impact behavior of the beams strengthened with KFRP laminates and steel plates. The beams externally strengthened with KFRP laminates performed well under impact loading, although they could not provide the same energy absorption as the beams externally strengthened with steel plates. They also concluded that additional anchoring at the ends of laminates would improve the impact resistance of these beams [1].

White, Soudki and Erki [2] also investigated experimentally the effects of strain rate on the behavior of reinforced concrete beams strengthened with CFRP laminates. Nine 3-m reinforced concrete beams, one un-strengthened and eight strengthened CFRP laminates were suddenly loaded. The stroke rates ranged from 0.0167 mm/s (slow loading rate) to 36 mm/s (fast loading rate). The rapidly loaded beams showed an increase of approximately 5% in capacity, stiffness, and

energy absorption. Ductility and the failure modes were not directly affected by loading rate changes [2].

Tang and Saadatmanesh [3] also tested a series of 27 concrete beams to investigate the behavior of concrete beams strengthened with FRP laminates under impact loading in the laboratory. Two out of the 27 beams were not retrofitted and were used as control specimens. They applied the impact force with a steel drop weight [3]. The conclusion was devoted to the fact that composite laminates bonded to concrete beams could significantly improve the serviceability of this type of structure to withstand impacts. In addition, bonding laminates increased cracking and flexural strength as well as residual stiffness of the beams. Furthermore, it reduced the number of cracks, crack widths and the maximum deflection [3].

**ANALYTICAL APPROACH**

In general, two types of response in a concrete beam under impact loading can be observed, that is local and global deformations. Local deformations are directly caused by the contact occurred between the projectile and beam surface, but global responses are caused by the dynamic vibration of the member. Because of the high intensity of global response rather than local deformations, in low velocity impacts, global deformations dictate the majority of principles related to the analysis and designation of impact resistance reinforced concrete beams. So, in analytical formulations, the global stiffness and deformation regime were taken into account. But, it should be mentioned that the global point of view must be correlated according to local effects [4].

**Impact Force**

In order to determine an elastic estimation of the impact force applied to a simply supported beam, an idealized spring-mass can be used. The analytical model is assumed as a two-freedom-degree system with a global elastic stiffness as shown in Figure 1. The dynamic motion equations of the total system can be

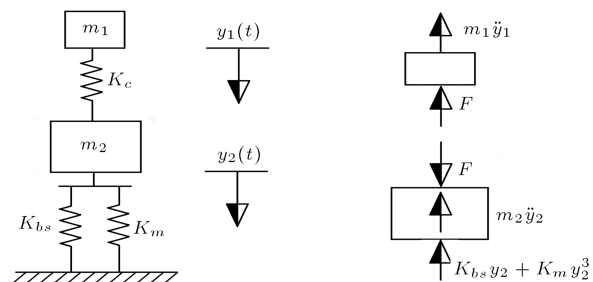


**Figure 1.** Spring-mass idealization of impact phenomenon.

expressed as the following relations:

$$\begin{aligned} m_1 \ddot{y}_1 + F &= 0, \\ m_2 \ddot{y}_2 + K_{bs} y_2 + K_m y_2^3 + F &= 0. \end{aligned} \tag{1}$$

Here,  $m_1$  and  $m_2$  are the masses of the projectile and beam, respectively;  $y_1$  and  $y_2$  are the displacements of the projectile and beam;  $F$  is the contact force between the projectile and beam;  $K_{bs}$  is the bending-shear stiffness of the beam; and  $K_m$  is the membrane stiffness. The initial conditions are expressed at  $t = 0$  (before contact):

$$\dot{y}(0) = V, \quad y_1(0) = y_2(0) = 0.0. \tag{2}$$

Hence,  $V$  is the initial velocity of the impactor just before contact occurs. If the axial deformation and the projectile indentation are assumed insignificant, the model may be considerably simplified to a single degree of freedom system with the following equation of motion:

$$m_1 \ddot{y} + K_{bs} y = 0. \tag{3}$$

For further simplification of the equilibrium equation, the effective mass of the structure is neglected. As a result, the structure and projectile will vibrate together as soon as the contact takes place.

$$y(t) = \frac{V}{\omega} \sin(\omega t), \quad \omega = \sqrt{K_{bs}/m_1}. \tag{4}$$

Because the contact force,  $F$ , is equal to the force in the linear elastic spring,  $K_{bs}$ , the contact force history can be expressed as follows:

$$F = \begin{cases} V\sqrt{K_{bs}m_1} \sin(\omega t) & \leftarrow \omega t \leq \pi \\ 0.0 & \leftarrow \omega t > \pi \end{cases} \tag{5}$$

The above equation is set based on the assumption that the beam stiffness remains constant during the impact. But, the stiffness of reinforced concrete beams decreases as it subjects under the crack failure. So, the impact force should be corrected with a reduction factor, like  $R_F$ , to incorporate the effects of reduced stiffness [4]. The impact force reduction factor will be estimated using the numerical inelastic dynamic analysis results.

**Deflection**

The governing equation of motion for a beam under impact loading can be developed using a flexural wave theory as the following equilibrium formula [5]:

$$\frac{\partial^2}{\partial x^2} \left( EI \frac{\partial^2 y}{\partial x^2} \right) + \rho A \frac{\partial^2 y}{\partial t^2} = q(x, t). \tag{6}$$

Here,  $y$ ,  $\rho$ ,  $A$  and  $EI$  are the beam displacement, density, section area and the elastic bending stiffness, respectively. The initial conditions of the differential equation are as follows:

$$\dot{y}(x, 0) = 0, \quad \ddot{y}(x, 0) = 0.$$

An explicit solution of the following boundary value fourth-order PDE problem needs a Laplace transformation to be applied. If the initial dynamic conditions are merged with the new obtained equation, the transformed equation can be expressed as follows [5]:

$$\frac{EI}{\rho A} \bar{y}^{(4)}(x, s) + s^2 \bar{y}(x, s) = \frac{\bar{q}(x, s)}{\rho A}. \tag{7}$$

As can be shown,  $s$ ,  $\bar{q}$  and  $\bar{y}$  are the transformed shape of time, load, and deflection parameters, respectively. Using the orthogonal infinite series, the expansion-based general solution of the equilibrium equation can be stated as follows [5]:

$$\begin{aligned} \bar{y}(x, s) &= \frac{2}{\rho Al} \sum_{n=1}^{\infty} \frac{Y_n(x)}{(a^2 \beta_n^4 + s^2)} \int_0^l \bar{q}(u, s) Y_n(u) du, \\ Y_n(x) &= \sin \frac{n\pi x}{l}, \quad \beta_n = \frac{n\pi}{l}. \end{aligned} \tag{8}$$

Here,  $l$  is the length of the beam and  $Y_n$ , and  $\beta_n$  are the orthogonal-type deflection and mode shapes of the vibrating beam. Using the inverse Laplace-transform function, one can obtain the real response of the beam as a function of its elastic stiffness, applied load and initial-boundary conditions as follows:

$$\begin{aligned} y(x, t) &= \frac{2}{\rho Al} \sum_{n=1,3,5}^{\infty} \frac{Y_n(x)}{a \beta_n^2} \\ &\left[ \int_0^l \int_0^t q(u, \tau) Y_n(u) \sin a \beta_n^2 (t - \tau) d\tau du \right], \end{aligned} \tag{9a}$$

$$\omega_n = a \beta_n^2 = \left( \frac{n\pi}{l} \right)^2 \sqrt{\frac{EI}{\rho A}}. \tag{9b}$$

Here,  $\omega_n$  is the  $n$ th-mode natural vibration frequency in radian/sec. The presented equation can calculate the closed-form elastic response of a simply supported beam subjected to any general time-dependent loading. Now, consider a case where the external load is an impact type and is applied at the beginning of the time domain. The impact load has total magnitude of  $P$  and is applied in the  $x_0$  location of the beam span. Considering the Dirac delta function, the mentioned load function can be expressed as follows [5]:

$$q(x, t) = P \delta(x - x_0) \delta(t). \tag{10}$$

Here,  $\delta(x - x_0)$  and  $\delta(t)$  are the Dirac delta functions of the impact force in the  $x_0$  location of the beam span and in the  $t = 0$  moment of the response time domain, respectively. By substituting the Laplace-transformed form of the Dirac delta force function into Equations 9 and doing some mathematical manipulation and simplifications, the final solution of the deflection equation can be expressed as below [5]:

$$y(x, t) = \frac{2P}{\rho Al} \sum_{n=1,3,5}^{\infty} \frac{(-1)^{(n-1)/2} \sin\left(\frac{n\pi x}{l}\right) \sin(\omega_n t)}{\omega_n}, \quad (11a)$$

$$P = \int_0^{\frac{\pi}{\omega}} V \sqrt{K_{bs} m_1} \sin(\omega t) dt, \quad \omega = \sqrt{\frac{K_{bs}}{m_1}}. \quad (11b)$$

Because of the inelastic response of the beam and its frequent cracking modes, the system will absorb more impact force and, then, may deflect less than its analytical value. So, the subsequent numerical deflection values will be less than the analytical ones and therefore analytical results should be scaled down with a reduction factor like  $R_D$  [5]. The maximum deflection reduction factor can be determined using the numerical inelastic dynamic analysis results and will be presented after the finite element analysis of the structure.

## MATERIAL CONSTITUTIVE MODELS

Materials used in the finite element analysis of reinforced concrete beams under projectile impact loading include steel reinforcing rebars, concrete, epoxy resin and FRP laminates. Many reliable and applicable constitutive material models are available in commercial finite element analysis source code libraries [6]. So, their input material properties and associated constitutive models have to be only introduced briefly. It is assumed that all materials, except unidirectional FRP laminates, will behave in an elastic, plastic and fracture nonlinear regime. FRP laminates almost behave in a linear elastic mode up to the rupture. The failure mode of stated composite laminates can be determined on the critical stress ratio of each failure mode for further investigations.

### Concrete

Under multi-axial combinations of loading, the failure strengths of concrete are different from those observed under uniaxial conditions. However, the case of a maximum strength envelope under multiaxial stress seems to be independent of the load path [7]. A Mohr-Coulomb type compression surface together with a crack detection surface is used to model the yield and failure surfaces of concrete as shown in Figure 2.

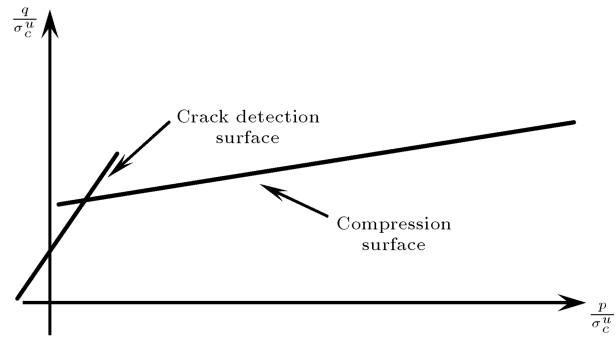


**Figure 2.** Schematic concrete failure surfaces in meridian-deviatoric plane.

If the principal stress components of concrete are compressive, the response of the concrete is modeled by an elastic-plastic theory with a non-associated flow rule and an isotropic hardening plasticity. In tension, once cracking is defined to occur (the crack detection surface criteria is satisfied), the orientation of the cracks in integration points are stored (non-rotating smeared crack theory). Damaged elasticity and fracture energy is used to model the mesh-independent cracking phenomenon [7].

Here,  $p$ ,  $q$  and  $\sigma_c^u$  are, respectively, the first invariant of the volumetric stress tensor, the second invariant of the deviatoric stress tensor, and the maximum uniaxial compressive failure stress. When the cracking of concrete takes place, a smeared model is used to represent the orthotropic macro-crack behavior. It is known that the cracked concrete element can still carry some tensile stress in the direction normal to the crack, which is termed as tension stiffening [7]. In this study, a simple linear elastic fracture-based damaged model proposed by Hillerborg & Břazant [8] is used to model this tension stiffening phenomenon. This method can also result in the mesh independency of the response and localization modeling. The cracking behavior can be represented by a stress-displacement relationship using fracture energy. It is assumed that the fracture energy required to form a unit area of the crack surface,  $G_f$ , is a material property. This value can be calculated from measuring the tensile stress as a function of the crack opening displacement. Typical values of  $G_f$  range from 40 N/m for a traditional construction concrete ( $f'_c = 20$  MPa) to 120 N/m for a high strength concrete ( $f'_c = 40$  MPa) [8]. A schematic view of a concrete fracture model is shown in Figure 3. The concrete material used in the numerical analysis had characteristic constants as stated in Table 1. These values were calibrated on the previous experimental tests and results [3].

Here the dilation angle,  $\psi_c$ , is the angle of the compression surface line in a  $p - q$  plane with respect to the  $p$  axis, and it can be accounted as the lateral confinement implementation parameter [7]. The strain

Table 1. Concrete material model input values.

<b>Elastic Modulus</b>	$E_c$	28240 (MPa)
<b>Poisson's Ratio</b>	$\nu_c$	0.19
<b>Density</b>	$\rho_c$	2402.77 (kg/m <sup>3</sup> )
<b>Compressive Strength</b>	$f'_c$	36.1 (MPa)
<b>Dilation Angle</b>	$\psi_c$	36.34 (degree)
<b>Biaxial to Uniaxial Failure Stress Ratio</b>	$\sigma_{b0}/\sigma_{c0}$	1.16
<b>Fracture Energy</b>	$G_f$	104.4 (N/m)

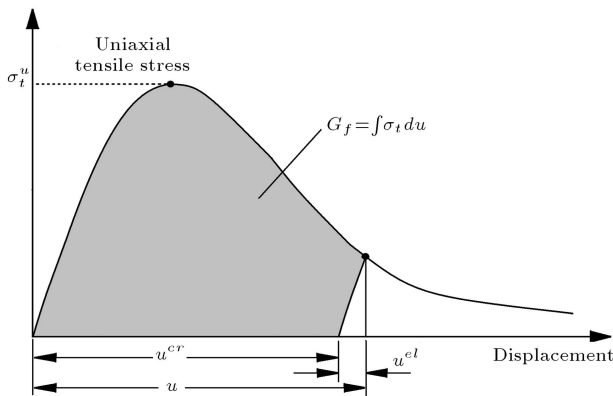


Figure 3. Crack formation based on fracture energy.

rate effect is also modeled by magnifying the maximum compressive strength and elastic modulus, and by decreasing the failure compressive strain. The semi-analytical modifying relations are presented by Břzant, Mander and Park [9]. The compressive strength of concrete becomes more sensitive by increasing the strain rate, rather than by any change in its elastic modulus. However, increasing the strain rate would result in a decrease of the compressive strength value. There is no significant change in the ultimate failure strain value of concrete in the uniaxial behavior. The strain rate effect in the uniaxial behavior of modeled concrete is shown in Figure 4.

**Steel Reinforcing Rebar**

The stress-strain curve of the reinforcing rebars (longitudinal and transverse) is assumed to be elastic, followed by a multi-linear kinematic hardening plasticity based on the von-Mises associated flow rule as shown in Figure 5. The steel reinforcements are treated as a two-node truss elements network embedded discretely in concrete brick elements, and the full bond effect between concrete and steel elements are imposed by integration points and nodal constrains. In order to properly model the constitutive behavior of the reinforcement, the cross sectional area, spacing and position of all reinforcements are exactly modeled in a finite element configuration of a three-dimensional

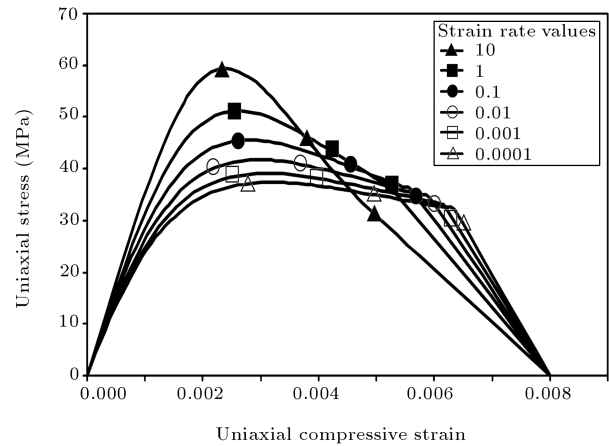


Figure 4. Strain rate effect on compressive uniaxial behavior.

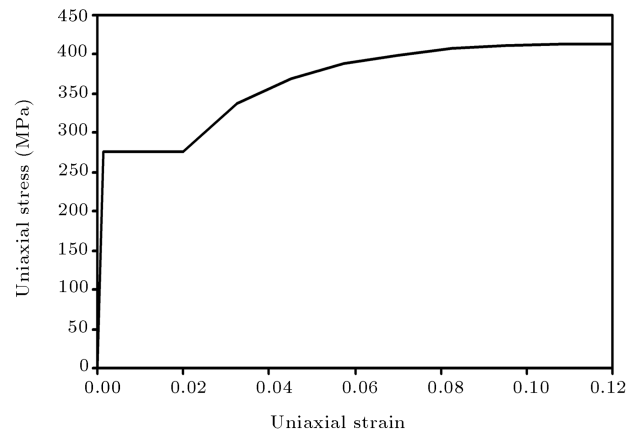


Figure 5. Elastic-hardening plastic uniaxial model for steel reinforcing bar.

reinforced concrete beam model. The steel material used in the numerical analysis was the ASTM A615 Grade 40 type, which had characteristic constants as stated in Table 2. Values are based on recent experimental tests and results [3].

**Fiber-Reinforced Polymeric Laminate (FRP)**

For fiber-reinforced polymers, each lamina can be considered as an orthotropic layer in a plane stress

**Table 2.** Steel material model input values.

<b>Elastic Modulus</b>	$E_s$	199947.98 (MPa)
<b>Poisson's Ratio</b>	$\nu_s$	0.29
<b>Density</b>	$\rho_s$	7849.05 (kg/m <sup>3</sup> )
<b>Yield Strength</b>	$f_y$	275.79 (MPa)
<b>Rupture Strength</b>	$f_u$	413.68 (MPa)
<b>Hardening Characteristic</b>	-	kinematic

condition. It is known that unidirectional fibrous composites behave elastically and linearly up to their failure criteria. It should also be mentioned that each lamina behaves isotropic in its transverse directions. The laminate used in this investigation is a unidirectional carbon based FRP laminate (CFRP) with the following material characteristics. These special type orthotropic materials have nine independent elastic constants. For simplification of the analysis process, the maximum stress of each failure mode had been used as the failure criteria of the unidirectional laminate (stress-based Rankin failure criteria). In Table 3,  $E$ ,  $G$ ,  $X$ ,  $Y$  and  $S$  present elastic modulus, shear modulus, fiber-direction strength, matrix-direction strength and shear strength of laminate in its local coordinates, respectively. Axis 1 is parallel to the fiber direction, axis 2 is the in-plane matrix direction and, finally, axis 3 is the out of plane matrix direction (normal).

### Epoxy Bonding Resin

Most high-strength bonding resins remain in the elastic linear zone up to their failure limit. But, in the post failure region, they soften linearly in a fractured procedure and their stiffness degrades. The stiffness in any part of the softening process depends on the dissipated fracture energy in the loading path. The limit behavior of the bonding resin consists of the following three stages:

1. Damage initiation,
2. Damage evolution,
3. Stiffness degradation.

This modeling method is proposed by Camanho and Davila in the National Aeronautic and Space Association, US (NASA) [10]. The assumed linear damaged elasticity model for bonding resin is quite similar to the fracture of concrete in tension. Resins used for mechanical and civil engineering purposes are mostly un-reinforced tough-epoxy and have an isotropic material configuration. The mechanical characteristics of the resin used in this investigation are stated in Table 4.

Here,  $E$ ,  $G_1$  and  $G_2$  are the elastic modulus normal to the bond interface and the shear modulus in two transverse directions in the bonding plane, respectively. It is assumed that the debonding phenomenon can be initiated from the mid-plane of the bonding interface thickness. For determination of the damage initiation limit, values like bond normal strength,  $N_0$ , and transverse bond shear strengths,  $T_0$  and  $S_0$ , should be checked according to interface existing stresses. For the damage evolution process, a fracture energy interactive criterion, called Benzeggah-Kenane, has been applied to the debonding problem [11]. In this criterion, the stiffness degradation of the normal and transverse behavior of resin is modified by the dissipated energy resulted from interface relative displacements. The degraded stiffness of the bonding resin can be obtained using the interface damage index,  $D$ , which is calculated from the recent deformed status of the interface [11].

## NUMERICAL APPROACH

### Geometry of Beams and FE Models

For investigation of a concrete beam, considering its nonlinear behavior under low velocity impact loading,

**Table 3.** CFRP laminate material model input values.

Plastic Modulus (MPa)		Poisson's Ratio		Mode-Failure Strengths (MPa)				Shear Modulus (MPa)		Shear Strength (MPa)	
				Tensile		Compressive					
$E_1$	144700	$\nu_{12}$	0.3	$X_T$	1240	$X_C$	870	$G_{12}$	5200	$S_{12}$	77
$E_2$	9650	$\nu_{13}$	0.3	$Y_T$	52	$Y_C$	230	$G_{13}$	5200	$S_{13}$	77
$E_3$	9650	$\nu_{23}$	0.45	$Y_T$	52	$Y_C$	230	$G_{23}$	3400	$S_{23}$	38

**Table 4.** Bonding epoxy resin material model input values.

Density (kg/m <sup>3</sup> )	Elastic Modulus (MPa)		Failure Strengths (MPa)		Fracture Energy (N/m)	
1260	E	4300	$N_0$	61	$G_n^C$	75
	$G_1$	1600	$T_0$	68	$G_t^C$	547
	$G_2$	1600	$S_0$	68	$G_s^C$	547

smear-plasticity based FE models were proposed and used for determination of the global and local response of beams. A constant regular discrete mesh is implemented for the numerical modeling. Furthermore, the constitutive relations of materials are formulated at the element integration points. To increase the efficiency of numerical results, the aspect ratio of elements are kept equal to one for solid concrete and epoxy resin materials. The dynamic responses of models are calculated using the central difference formulation of structural motion equations. In the numerical analyses, sixteen simply supported reinforced concrete beams with various stiffness and impact energy levels, are considered. It should be mentioned that the shear deformation is more pronounced in short beams rather than long ones and, so, the shear stiffness of all models should be considered in analytical solutions. To study the influence of retrofitting laminates, the minimum allowed ACI 318-08 code (specified shear and flexural reinforcement ratios) is considered in the proposed models [12]. For the concrete core continuum, an eight-node brick element (C3D8) has been used that can consider nonlinear geometrical effects, plasticity and damaged deformations. Three orthogonal crack planes are accounted for in all integration points of the brick element. The tensile behavior of the concrete is implemented by the damaged-elasticity fractured model.

For retrofitting CFRP laminates, a four-node shell element (S4) with a composite lay-up section is used for the finite element simulation of strengthened models. A plane stress condition is assumed in the constitutive relations of each lamina stiffness relation. CFRP laminates are tied to epoxy resin elements at the top and bottom surfaces of beams and are of unidirectional 0.5-mm thickness, CFRP T300/977-2, in type.

The bonding resin interface is also modeled with an eight-node cohesive element (COH3D8) with four integration points in its mid-plane interface. Resin elements are merged with laminate shell elements and concrete brick elements in the flexural surfaces of beams. A traction-separation constitutive relation combined with a Benzeggah-Kenane fracture energy model is used in the simulation of the resin interface debonding. The bonding interface has a 2-mm thick M10 epoxy resin material property.

Modeled RC beams with simply supported boundary conditions are in a rest status (zero velocity initial condition). Before applying the impact, models are statically analyzed to gravitational loading. Then, a 22.73 - kilogram steel cylinder is dropped freely from 1 and 1.5 meter heights to the top surface of beams repeatedly. The location of the dropping is assumed in the beam midspan for maximum deflection. For numerical simplification of models, only one quarter of each beam is modeled as a result of symmetric

boundary conditions. Regarding the higher stiffness value of steel rather than concrete, the projectile is modeled by discrete rigid 3D elements. The contact between the projectile and beam is considered as a hard contact. Therefore, the resultant contact force will incrementally be calculated in the time domain by taking into account projectile penetration and beam deformation. The typical FE model idealization is shown in Figures 6 and 7.

The rigid body formulation of the projectile contact zone is defined by the penalty contact method. The projectile is assumed to have no frictional contact and can be separated after completion of the penetration. The proposed models are categorized into two unretrofitted concrete beams (initiated with a S symbol) and laminate-retrofitted concrete beams (initiated with a R symbol). The geometrical and impact properties of beams used in this study are presented in Table 5. All concrete beams are 12 centimeters in width.

Minimum required flexural - shear reinforcement ratio rebars are calculated according to the ACI 318-08 structural code [12] as steel reinforcing rebars. The retrofitting capability of CFRP unidirectional laminates can be revealed well, if the minimum required reinforcement is provided. Models are loaded uniformly with their gravitational weights first and analyzed statically. The deformed and stressed models are then stroked by a falling drop projectile in the middle zone of their span. The nonlinear dynamic analysis period

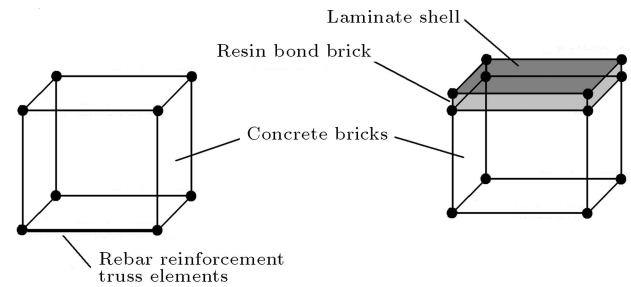


Figure 6. Finite element mesh configuration and connectivity.

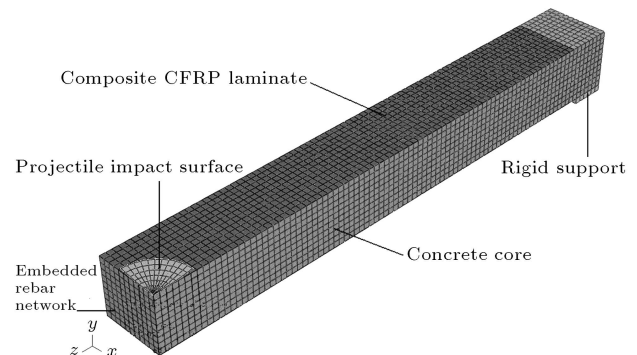


Figure 7. Idealization of simply supported concrete beams under impact loading.

**Table 5.** Properties of concrete beams used and their reinforcement details.

Model	Steel Rebar Reinforced	CFRP Retrofitted	Projectile Prop Height (m)	Beam Height (cm)	Span Length (m)	Rebar	Stirrups
S1h1L1	✓	×	1.0	10	1.6	4Φ6	2Φ4@40 mm
S1h1L2	✓	×	1.0	10	2.0	4Φ6	2Φ4@40 mm
S1h2L1	✓	×	1.0	16	1.6	4Φ8	2Φ4@80 mm
S1h2L2	✓	×	1.0	16	2.0	4Φ8	2Φ4@80 mm
S2h1L1	✓	×	1.5	10	1.6	4Φ6	2Φ4@40 mm
S2h1L2	✓	×	1.5	10	2.0	4Φ6	2Φ4@40 mm
S2h2L1	✓	×	1.5	16	1.6	4Φ8	2Φ4@80 mm
S2h2L2	✓	×	1.5	16	2.0	4Φ8	2Φ4@80 mm
R1h1L1	✓	✓	1.0	10	1.6	4Φ6	2Φ4@40 mm
R1h1L2	✓	✓	1.0	10	2.0	4Φ6	2Φ4@40 mm
R1h2L1	✓	✓	1.0	16	1.6	4Φ8	2Φ4@80 mm
R1h2L2	✓	✓	1.0	16	2.0	4Φ8	2Φ4@80 mm
R2h1L1	✓	✓	1.5	10	1.6	4Φ6	2Φ4@40 mm
R2h1L2	✓	✓	1.5	10	2.0	4Φ6	2Φ4@40 mm
R2h2L1	✓	✓	1.5	16	1.6	4Φ8	2Φ4@80 mm
R2h2L2	✓	✓	1.5	16	2.0	4Φ8	2Φ4@80 mm

of each beam was about 0.1 seconds and the minimum value of the time increment was about 5.81e-9 seconds.

In impact problems, the wave propagation velocity is much higher than the deformation velocity of the structure. Therefore, the time increment in the analysis should be taken quite small, so that the dynamic explicit solution of the structure approaches to an appropriate convergence. The time history of midspan deflection, total reaction force, cracking mode of RC beams, yielded zones of steel reinforcements and the probable debonding interfaces of resin are taken as output data.

**RESULTS AND DISCUSSION**

**Deflection of Models Under Impact Loading**

The average of the midspan node displacement is taken as the maximum midspan deflection. The general time history of the midspan deflection for beams S1h1L2, S2h2L1, R1h1L2 and R2h2L1 are plotted in Figures 8 to 11.

The damage rate of a S2h2L1 reinforced concrete beam is seen higher than beam S1h1L2. Also, vibration of the stiffer RC beam is damped more quickly than the softer one. The S1h1L2 beam vibrated when stroked for the third time, but the stiffer beam, S2h2L1, rapidly damped after some few vibrations. The rapid damping of vibrations in the S2h2L1 beam resulted in severe damage. It should be mentioned that the natural

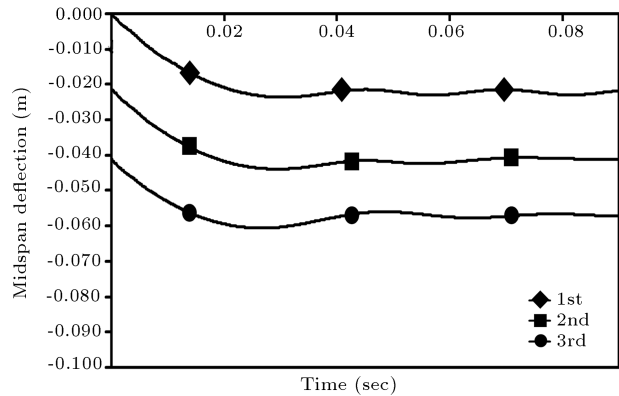


**Figure 8.** Deflection of S1h1L2 for first, second and third impact.

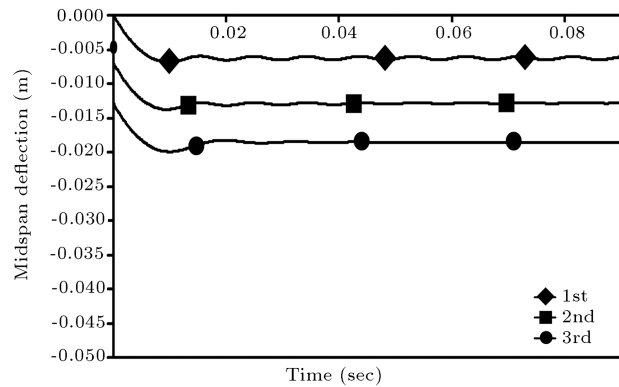


**Figure 9.** Deflection of S2h2L1 for first, second and third impact.

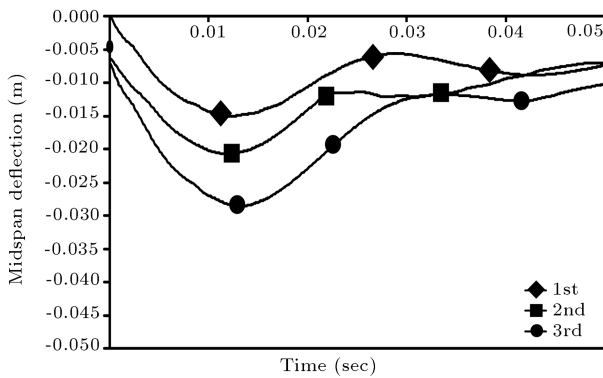


**Figure 10.** Deflection of R1h1L2 for first, second and third impact.

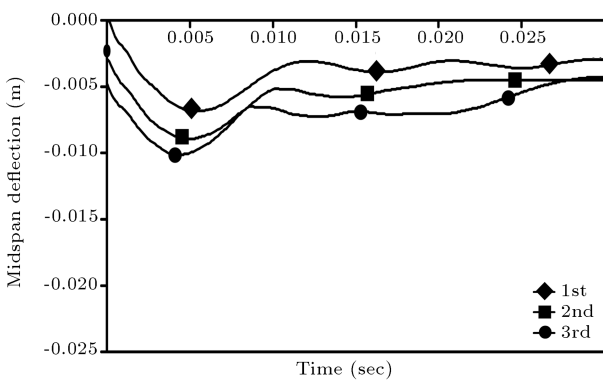


**Figure 11.** Deflection of R2h2L1 for first, second and third impact.

damping of reinforced concrete beams depends on their plastic deformations and their concrete cracking modes. Beams that are vibrated well in their flexural modes can dissipate the imposed impact energy as a cracking and crushing formation. Therefore, beams with higher values of stiffness and little plastic deformation capability may receive more impact load and can then undergo more damage. The analytical and numerical maximum deflection values of all analyzed beams are reported in Table 6.

The retrofitting effect of CFRP laminate can be easily shown by comparing Figures 9 and 11. FRP laminates have controlled the variation domain of the deflection in its transient and steady state response zone. CFRP-retrofitted reinforced concrete beams had much lower maximum deflection values and also had a special convergence in residual deflection values in all impact repeats. It shows that FRP laminates can distribute the local deformations to a wider range of the beam span and take the contribution of the whole beam for controlling the impacted zone deflection of the structure. Continuity effects of composite laminates were valid for all analyzed models. But, the deflection controlling effect was more apparent in long low-depth (flexure controlled) reinforced concrete beams. By increasing the impact energy level, the

average deflection value of concrete beams is increased, but FRP laminates constantly reserved their deflection controlling effect in these cases too. Furthermore, the analytic mathematical method resulted in higher values of deflection with respect to the numerical method as a result of the severe inelastic behavior of beams.

**Reaction Force**

A reaction force response occurred more rapidly than the deflection response. The summation of end support reaction forces is taken as the total impact-induced reaction force. It is obvious that the time history variation of the reaction force depends on reduced stiffness, impact energy level, type of beam (long low-depth or short high-depth) and reinforcement ratio (steel rebar and FRP). The time history response of the beams, S1h1L2, S2h2L1, R1h1L2 and R2h2L1, are plotted in Figures 12 to 15. It is revealed that the maximum value of the reaction force (absorbed impact force) is decreased by increasing the impact applying times. This is due to the stiffness degradation of the structure as a result of damage evolution.

It can be observed that the beams with lower stiffness values absorbed less impact force (reaction

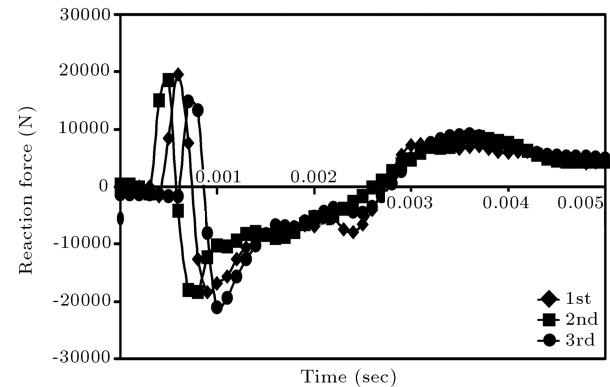


**Figure 12.** Reaction force of S1h1L2 for first, second and third impact.

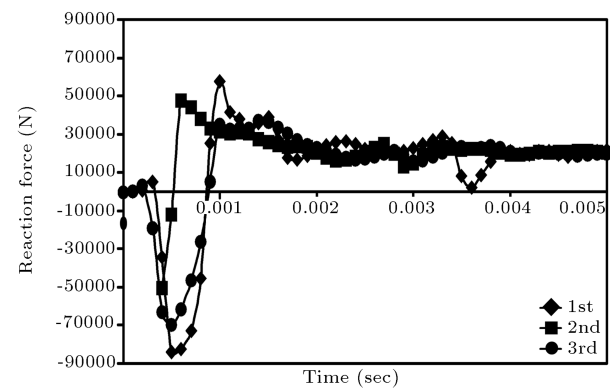


**Figure 13.** Reaction force of S2h2L1 for first, second and third impact.

**Table 6.** Maximum deflection values of analyzed reinforced concrete beams.

Model	Stiffness (N/m)	Analytical (N)	Numerical (N)	Ratio ( $R_D$ )
S1h1L1	3.51E+06	26.04	18.49	1.408
S1h1L2	1.80E+06	32.55	23.63	1.378
S1h2L1	1.48E+07	9.93	6.78	1.465
S1h2L2	7.68E+06	12.41	8.53	1.455
S2h1L1	3.51E+06	31.89	20.12	1.585
S2h1L2	1.80E+06	39.86	25.47	1.565
S2h2L1	1.48E+07	12.16	7.46	1.630
S2h2L2	7.68E+06	15.20	9.52	1.597
R1h1L1	4.02E+06	24.34	14.02	1.736
R1h1L2	2.06E+06	30.42	19.91	1.528
R1h2L1	1.61E+07	8.54	4.48	1.908
R1h2L2	8.32E+06	11.91	6.25	1.905
R2h1L1	4.02E+06	29.81	15.85	1.880
R2h1L2	2.06E+06	37.26	22.42	1.662
R2h2L1	1.61E+07	10.46	5.18	2.021
R2h2L2	8.32E+06	14.59	7.29	2.001

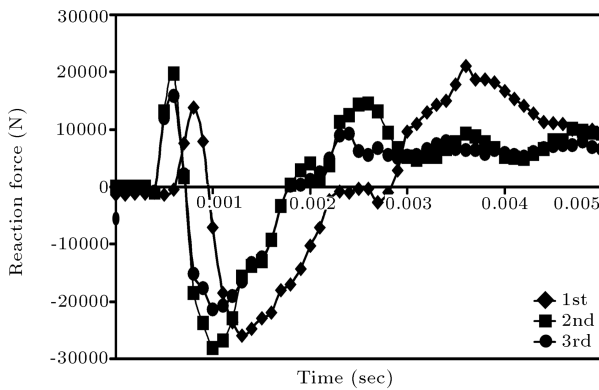


**Figure 14.** Reaction force of R1h1L2 for first, second and third impact.

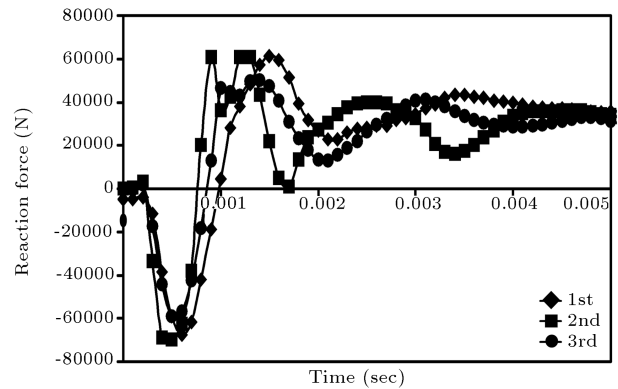


**Figure 15.** Reaction force of R2h2L1 for first, second and third impact.

force) than those with higher ones. These beam types also had less reaction force variation during their steady state time domain. Beams with high stiffness values lost a major proportion of their load carrying capacity during the second and third impacts in comparison with lower stiffness beams. This phenomenon implies that RC beams with higher stiffness values may be damaged more severely under impact loading than lower stiffness ones. In other words, the impact-induced damage rate of a RC beam is proportional to its stiffness value. It also should be mentioned that an increase in the impact energy level can result in an increasing of the reaction force and a reduction in the beam stiffness. The analytical and numerical results of the maximum reaction force are stated in Table 7.

By analyzing Figures 14 and 15, it can be easily seen that retrofitted RC beams showed less reaction

force variations and also preserved their impact load carrying capacity in their transient and steady state dynamic responses. The response-continuity effect of CFRP laminates has increased the impact load carrying capacity of retrofitted beams too. The difference between analytical and numerical reaction force results is directly affected by increasing the impact energy level. But, retrofitting concrete beams reduces these differences and addresses a global behavior rather than a local response to retrofitted members. This is a positive effect produced by FRP laminates.

Comparing Tables 6 and 7, one can see that the analytical-numerical reaction force differences are much less than deflection differences. In retrofitted beams, this result gap is more apparent. This shows that CFRP laminates work as a deflection-reducer rather than an impact force-absorber. With lower failure

**Table 7.** Maximum reaction force values of analyzed reinforced concrete beams.

Model	Stiffness (N/m)	Analytical (N)	Numerical (N)	Ratio ( $R_F$ )
S1h1L2	3.51E+06	39490.70	27332.56	1.445
S1h1L1	1.80E+06	28308.00	19292.07	1.467
4S1h2L2	1.48E+07	81198.25	54984.38	1.477
S1h2L1	7.68E+06	58377.68	39363.68	1.483
S2h1L2	3.51E+06	48366.04	30192.27	1.602
S2h1L1	1.80E+06	34670.07	21215.84	1.634
S2h2L2	1.48E+07	99447.14	59203.44	1.680
S2h2L1	7.68E+06	71497.76	41621.53	1.718
R1h1L2	4.02E+06	42223.32	29460.05	1.433
R1h1L1	2.06E+06	30274.60	20927.10	1.447
R1h2L2	1.61E+07	84519.59	58064.51	1.456
R1h2L1	8.32E+06	60789.81	41577.67	1.462
R2h1L2	4.02E+06	51712.79	32626.02	1.585
R2h1L1	2.06E+06	37078.66	22852.00	1.623
R2h2L2	1.61E+07	103514.93	62475.37	1.657
R2h2L1	8.32E+06	74452.01	44101.16	1.688

deflection, the system can withstand more ultimate impact forces, so, these two retrofitting criteria are not independent and are somehow related to each other.

**Impact-Induced Cracking and Failure Modes**

After applying the third impact, the cracks in the concrete core and yielded zones of the reinforcement network were appeared. The debonding probable interface zones, resin damage index distribution and strength status of the CFRP laminate are also investigated. Two types of concrete cracking mode are observed in reinforced concrete beams under impact:

1. Flexural cracks,
2. Shear cracks.

In intact beams, flexural cracks are localized in the impacted zone of the beam and resulted in the local yielding of longitudinal rebars. But, for the retrofitted beams, flexural cracks are distributed in a wider range of concrete beams and, therefore, resulted in an increase of yielded rebar lengths. CFRP laminate also controlled the depth and width of flexural cracks in all models and reduced the local effect of the induced impact. The cracking modes and yielded zones of steel rebars are plotted in Figures 16 to 19. The crack modes in retrofitted concrete beams are different from intact ones. The number and depth of cracks are dependent on the beam type (long or short) and the impact energy level.

By comparing Figures 16 and 18, it can be concluded that CFRP laminates made results in a wider

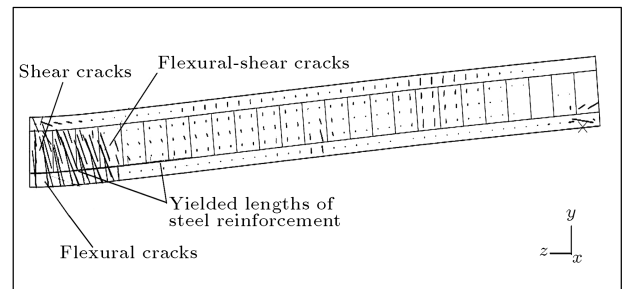


**Figure 16.** Concrete crack distribution and steel rebar yield mode of S1h1L2.

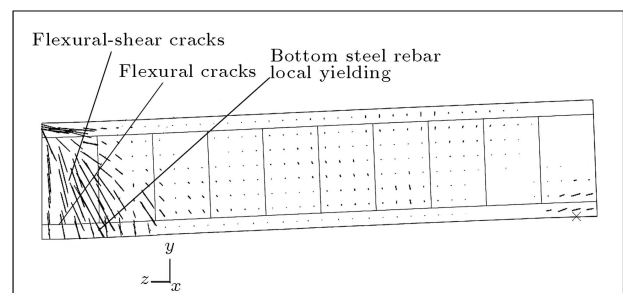


**Figure 17.** Concrete crack distribution and steel rebar yield mode of S2h2L1.

distribution of flexural cracks and, finally, increased the ductility of the ultimate failure of members. Global responses are more desirable than local deformations and are taken into account in the designation of structural members. FRP laminate assists the global response in becoming more apparent. The CFRP laminate also made the top longitudinal steel rebar become locally yielded. The important thing to notice is that in long and low-depth RC beams, there are some

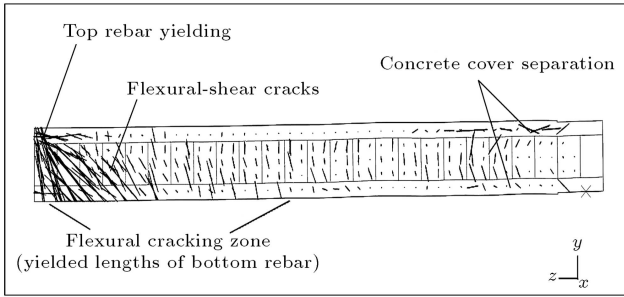


**Figure 18.** Concrete crack distribution and steel rebar yield mode of R1h1L2.

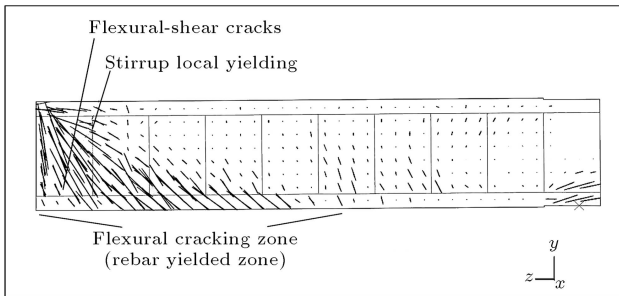


**Figure 19.** Concrete crack distribution and steel rebar yield mode of R2h2L1.

local longitudinal cracks concentrated at the ends of the beam in laminate cutoff zones. These cracks are distributed in concrete cover zones and can result in the separation of this part. This failure case is not revealed well in short high-depth reinforced concrete beams.

The CFRP laminate also was efficient in the better distribution of flexural and shear concrete cracks of short high-depth beams (compare Figures 17 and 19). Shear cracks are occurred more in these types of beam. However, it can easily be verified that CFRP laminate was more controlling on long low-depth beams than the mentioned short high-depth beams. The composite laminate-based retrofitting of reinforced concrete beams made the flexural cracks become slightly declined due to the constrain influence of the laminate in controlling the strain values of the retrofitted beam. The impact energy level increase made the cracks be redistributed wider and deeper. It also made the local stirrups to be yielded in the impacted zone.

**Bonding Interface Status**

The bonding interface strength and damage status was also investigated in this study. Considering the debonding probability, retrofitted reinforced concrete beams with lower stiffness were more critical than beams with higher values of stiffness. It was shown that longer beams with lower depth are so sensitive to debonding phenomenon and this is due to more

flexural cracked zones of the concrete interface. The main effect of CFRP laminate was established very well when the concrete cracks and the local internal force is transmitted to composite laminate. Debonding of the CFRP laminate will be initiated where the damage index reaches the critical value one. If the damage index of the bonding resin is equal to one, it means that no more interfacial stresses could carry on and, therefore, the interfacial stiffness approaches to zero. The NASA proposed constitutive model was quite exact with regard to experimental results driven by recent investigations [11]. The bonding interface damage index of the retrofitted concrete beams, R1h1L2 and R2h2L1, were plotted in Figures 20 and 21.

The debonding probable zones of the resin interface were located in the midspan and end support of the concrete beams. Consequently, the safe zone of the bond interface was located in the first quarter and third-quarter of the beam span. Because of local

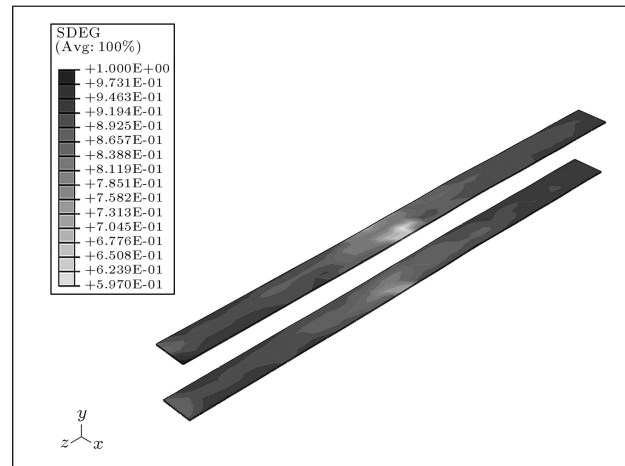


**Figure 20.** Bonding resin damage distribution contours of R1h1L2.

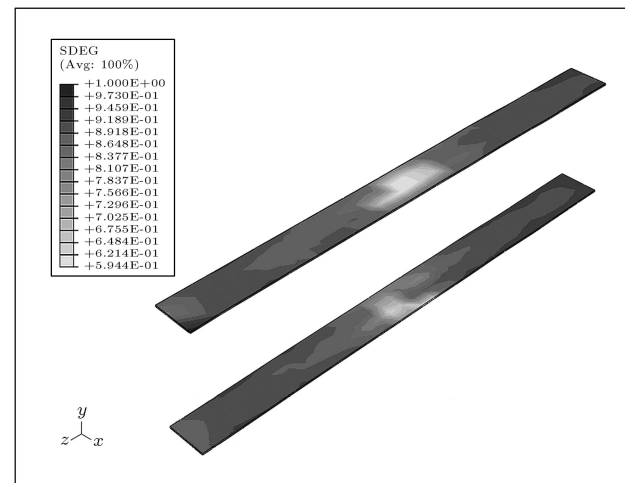


**Figure 21.** Bonding resin damage distribution contours of R2h2L1.

effects of the impact projectile, the top interface of the beam was more critical than the bottom interface at the midspan location. But, in general, on behalf of flexural cracks at the bottom surface, this interface is more likely to debond than the top interface at any location of the beam span. The damage index variation in beams with lower stiffness is much higher than high-stiffness beams. It is also proposed that the cutoff zones of the CFRP laminate at the end beam supports should be anchored to the beam in order to prevent laminate debonding (matrix cracking) or local concrete cover separation. It can easily be proved that the damage index values of the interface are getting more critical by increasing the impact energy level.

**VARIATION OF BEAM RESPONSES**

Considering the numerical and analytical results obtained from the dynamic analysis of the models, the variations of the maximum reaction force, maximum deflection and the stiffness variation of beams can be investigated. If the residual stiffness and deflection of retrofitted reinforced concrete beams were in the allowed service range, the remained strength of the member can be considered acceptable for further applied impact loads. The maximum reaction force variation is plotted with respect to the stiffness variation for two intact and retrofitted beam categories in Figure 22. It is clear that for a constant value of stiffness, a retrofitted beam will tolerate more impact load than a virgin one. Also, there is a little difference in the load capacity ranges of simple and retrofitted reinforced concrete beams.

The maximum midspan deflection variation is also plotted as a function of the beam stiffness for intact and retrofitted beam categories in Figure 23. Considering the maximum midspan variation with respect to stiffness, one can conclude that for lower values of stiffness, the CFRP laminate was more efficient in

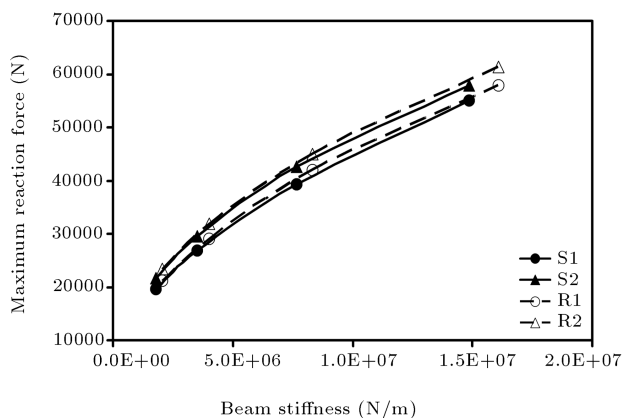


**Figure 22.** Maximum reaction force variation with regard to beam stiffness.

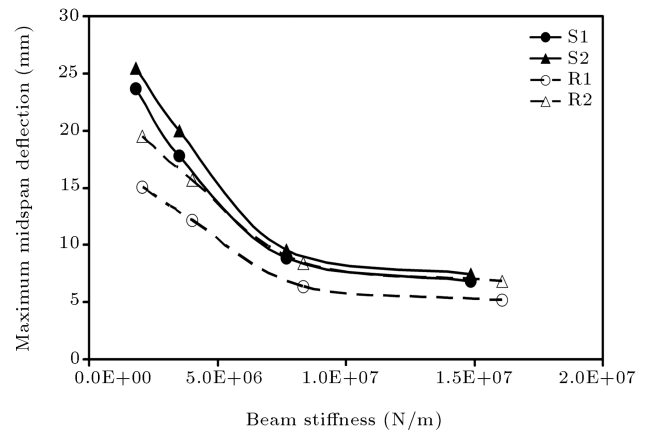


**Figure 23.** Maximum midspan deflection variation with regard to beam stiffness.

controlling the maximum deflection. The stiffness of reinforced concrete beams has a critical value and for values higher than this limit, the deflection reduction factor of retrofitted beams converges to a constant value. It should be stated that in retrofitted beams, the maximum deflection value is more sensitive to the impact energy level.

Stiffness variations of intact and retrofitted RC beams are plotted in Figures 24 and 25. Comparing these figures, one can deduce that unretrofitted beams are more sensitive to the times when the projectile was dropped onto the beam. Unretrofitted beams with a lower stiffness lost a major part of their stiffness at the moment of impact energy increase. Unretrofitted short beams resisted reserving their stiffness at first and second impacts, but finally lost a major part of their stiffness at the third impact.

It is verified that the laminate based retrofitting procedure is more effective in beams with higher lengths and lower depths. Retrofitted beams showed a much different performance compares to the intact ones. Retrofitted beams with higher stiffness reserved

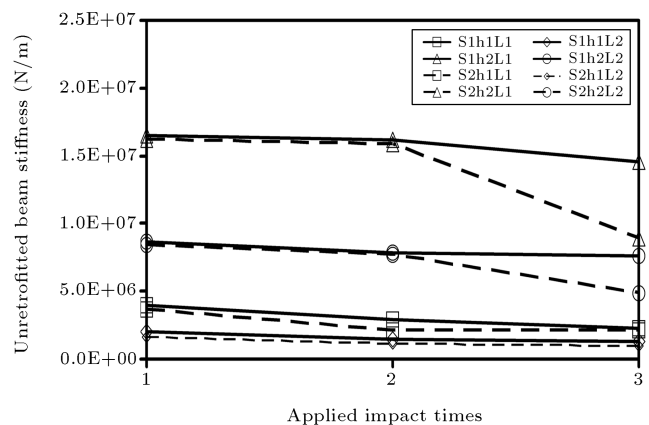


**Figure 24.** Stiffness degradation of intact concrete beam with respect to impact times.

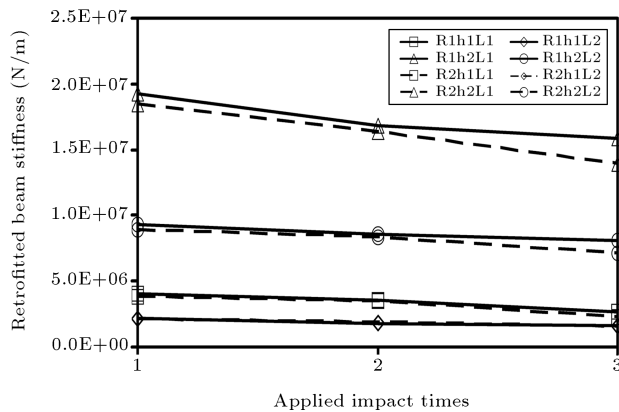


**Figure 25.** Stiffness degradation of retrofitted concrete beam with respect to impact times.

their stiffness in a much desired manner, rather than unretrofitted ones at all impact times.

## CONCLUSIONS

The impact effects on concrete beams strengthened with CFRP unidirectional composite laminates were studied thoroughly. The following conclusions are drawn based on the obtained results through analytical and numerical studies:

1. The retrofitting technique of RC beams using epoxy-bonded CFRP laminates can ensure the interface integrity and global deformation of members under impact loading.
2. Composite laminates increase the beam initial and residual stiffness. CFRP laminates also decreased the maximum deflection values and increased the maximum impact loading capacity.
3. CFRP laminate made the final failure mode of the retrofitted beam more ductile by increasing the number of flexural-shear cracks and extending the yielded lengths of steel rebar reinforcements.
4. For long low-depth reinforced concrete beams, a CFRP cutoff concrete cover separation failure mode is highly probable. Therefore, an FRP anchoring technique in this zone is highly recommended.
5. FRP-based retrofitting techniques are more likely to control the maximum deflection of a member than controlling the maximum absorbed impact force.
6. Long span low depth beams have more flexural cracks than shear cracks. However, the produced cracks in short span high-depth beams are almost in a shear mode. Thus, in long beams, the debonding status of the laminate bond interface is more critical than for short ones.
7. Unretrofitted RC beams having higher values of initial stiffness and induced impact energy were more

heavily damaged than similar beams with lower values of impact energy and stiffness. Retrofitted beams with similar cases were damaged less than intact ones.

## REFERENCES

1. Erki, M.A. and Meier, U. "Impact loading of concrete beams externally strengthened with CFRP laminates", *Journal of Composites for Construction*, pp. 3645-3659 (August 1999).
2. White, W.T., Soudki, A.K. and Erki, M.A. "Response of RC beams strengthened with CFRP laminates and subjected to a high rate of loading", *Journal of Composites for Construction*, pp. 153-162 (August 2001).
3. Tang, T. and Saadatmanesh, H. "Behavior of concrete beams strengthened with fiber-reinforced polymer laminates under impact loading", *Journal of Composites for Construction, ASCE*, **7**(3), pp. 65-67 (August 2005).
4. Krauthammer, T. "Blast mitigation technologies: Development and numerical considerations for behavior assessment and design", *Structures under Shock and Impact*, Computational Mechanics Publications, pp. 1-12 (1998).
5. Brillouin, L., *Wave Propagation and Group Velocity*, Academic Press, New York (1960).
6. Abaqus Inc., ABAQUS 6.7 User's Manual, SIMULIA, USA (2007).
7. Břazant, Z.P. "Concrete fracture models: Testing and practice", *Engineering Fracture Mechanics*, **69**, pp. 165-205 (2002).
8. Hillerborg, A., Modeer, M. and Peterson, P.E. "Analysis of crack formation and crack growth in concrete by means of fracture mechanics and finite elements", *Cement and Concrete Research*, **6**, pp. 773-782 (1976).
9. Mander, J.B., Priestley, M.J.N. and Park, R. "Theoretical stress-strain model for confined concrete", *Journal of Structural Engineering, ASCE*, **114**(8), pp. 1804-1825 (August 1990).
10. Camanho, P.P. and Davila, C.G. "Mixed-mode decohesion finite elements for the simulation of delamination in composite materials", *NASA/TM-2002-211737*, pp. 1-37 (2002).
11. Benzeggagh, M.L. and Kenane, M. "Measurement of mixed-mode delamination fracture toughness of unidirectional glass/epoxy composites with mixed-mode bending apparatus", *Composites Science and Technology*, **56**, pp. 439-449 (1996).
12. ACI "Building code requirements for structural concrete (ACI 318-08) and commentary", American Concrete Institute, Farmington Hills, MI 48331, USA (2008).